NIH Public Access
Author Manuscript
J Photochem Photobiol A Chem. Author manuscript; available in PMC 2014 June 10.

Published in final edited form as:
J Photochem Photobiol A Chem. 2012 November 15; 248: 24–29. doi:10.1016/j.jphotochem.2012.07.012.

Energy Transfer of CdSe/ZnS Nanocrystals Encapsulated with Rhodamine-Dye Functionalized Poly(acrylic acid)

Rebecca C. Somers[1], **Preston T. Snee**[2], **Moungi G. Bawendi**[1,*], and **Daniel G. Nocera**[1,*]

[1]Department of Chemistry, Massachusetts Institute of Technology, 77 Massachusetts Avenue, Cambridge, MA, 02139-4307

[2]Department of Chemistry, University of Illinois at Chicago, 845 West Taylor Street, MC 111, Chicago IL, 60607

Abstract

Energy transfer between a CdSe/ZnS nanocrystal (NC) donor and a rhodamine isothiocyanate (RITC) acceptor has been achieved via a functionalized poly(acrylic acid) (PAA) encapsulating layer over the surface of the NC. The modification of PAA with both *N*-octylamine (OA) and 5-amino-1-pentanol (AP), [PAA-OA-AP], allows for the simultaneous water-solubilization and functionalization of the NCs, underscoring the ease of synthesizing NC-acceptor conjugates with this strategy. Photophysical studies of the NC-RITC constructs showed that energy transfer is efficient, with k_{FRET} approaching 10^8 s^{-1}. The ease of the covalent conjugation of molecules to NCs with PAA-OA-AP coating, together with efficient energy transfer, makes the NCs encapsulated with PAA-OA-AP attractive candidates for sensing applications.

INTRODUCTION

Inorganic semiconductor nanocrystals (NCs) have generated considerable interest as fluorophores owing to their size-dependent physical properties caused by quantum confinement.[1–3] Broad absorption, narrow and tunable emission, high quantum yields, high two-photon absorption cross-sections and appreciable photostability are all properties that engender the utility of NCs for bioimaging applications.[4–11] The translation of NCs from imaging agents to sensing agents has been enabled by exploiting fluorescence resonance energy transfer (FRET) as a signal transduction mechanism between an analyte-sensitive fluorophore and the NC.[2,12–20] The confluence of NC photophysical properties and surface derivatization methods has opened the way for the development of NC-conjugates for bio-sensing[18,21–24] and cellular sensing applications.[25,26] The linchpin for NC sensing for these applications is the development of coatings for surface derivatization of the NC that do not affect the photophysical characteristics of the NC, have minimal affect on the NC hydrodynamic radius, and minimize the non-specific binding of the NCs to cellular and other biological structures.

nocera@mit.edu (D.G.N.); mgb@mit.edu (M.G.B.).

SUPPLEMENTARY MATERIALS

Full experimental details, gel permeation and FTIR characterization of modified poly(acrylic acid), and time-resolved decay traces of NCs and NC-dye conjugates available as Table S1, Figures S1 – Figure S3.

NIH-PA Author Manuscript
NIH-PA Author Manuscript
NIH-PA Author Manuscript

NIH-PA Author Manuscript

NIH-PA Author Manuscript

NIH-PA Author Manuscript

Most sensing applications, and especially those pertaining to biology, require water solubility of the NC construct. Therefore the hydrophobic coordinating ligands needed for NC sythesis must be altered to present a hydrophilic interface. In addition to imparting water solubility, NC coatings should preserve high quantum yields, provide functional handles for covalent conjugation of sensing active sites, offer long-term stability in aqueous solutions and allow for facile and large scale synthesis. Methods for water-soluble NCs include encapsulation via modifications with a layer of silica shell[4] or amphiphilic polymers,[9.27–29] or by directly exchanging the hydrophobic ligands with thiols,[5,30] phospholipids,[31] dendrimers,[32] or oligomeric phosphines.[33] Our group and others[34–37] have demonstrated increased interaction of thiol ligands with NCs by exploiting the multidentate binding motifs to furnish a new class of aqueous modified NCs that are compact, biocompatible, derivatizable and exhibit very low nonspecific binding. These same desirable properties for NC coatings has also been preserved for multidentate polyimidazole ligands[38] with the advantage that they overcome the long term chemical instability attendant to thiols.

We now describe a new amphiphilic polymer coating for the encapsulation of NCs that is also chemically robust over long time periods. Poly(acrylic acid) is modified with 5- *N*-octylamine and amino-1-pentanol (PAA-OA-AP) to allow for simultaneous water-solubilization and functionalization of the NCs. Steady-state and time-resolved spectroscopic investigations of RITC dye acceptor conjugate to the new NC scaffold establishes that the new coating can support FRET-based signal transduction for sensing applications

MATERIALS AND METHODS

All CdSe NCs overcoated with ZnS were prepared using a modified literature methods.[39–41] Poly(acrylic acid) was functionalized by coupling a fraction (40%) of the carboxylic acid groups of a 1800 MW poly(acrylic acid) (2.0 g, 0.0011 mol) with *N*-octylamine (1.44 g, 0.0110 mol) using 1-ethyl-3-(3-dimethylaminopropyl)carbodiimide (EDC) (2.12 g, 0.0110 mol) in *N*,*N*-dimethylformamide according to a previous report.[9] An additional 40% of the acid groups were coupled to vacuum-distilled 5-amino-1-pentanol (1.13 g, 0.0110 mol) using EDC (2.12 g, 0.0110 mol) in DMF, while the remaining 20% was left as free carboxylic acid. The functionalized polymer was purified by size-exclusion chromatography using Sephadex LH-20 with methanol as the mobile phase.

Four individual samples of dye conjugated polymer coated NCs were prepared by introducing controlled amounts of RITC (3.0 mg, 5.6 μmol; 0.30 mg, 0.56 μmol; 0.060 mg, 0.11 μmol; 0.030 mg, 56 nmol) to the PAA-OA-AP coated CdSe/ZnS NCs. The conjugates were purified by dialysis. After multiple washings, the free dye was completely removed from the NC-dye construct by dialysis as verified by the absence of the parent dye absorption features in the UV-vis absorption spectrum of the filtrate.

Quantum yield (Φ) measurements were using rhodamine 590 in ethanol as a reference (Φ_{ref} = 0.95[42]). A 400-nm emitting Ti:Sapphire laser equipped with a gated intensified CCD camera was used to obtain time-resolved fluorescence spectra.

NIH-PA Author Manuscript

NIH-PA Author Manuscript

NIH-PA Author Manuscript

Details of synthesis and measurements are provided in Supporting Information.

RESULTS AND DISCUSSION

PAA-OA-AP amphiphilic polymer on NCs

Micellar, amphiphilic, encapsulated NCs are superior to cap-exchanged NCs because replacement of the surface passivating organic groups during cap exchange drastically reduces NC quantum yields. Additionally, cap-exchanged NCs are not as stable over time as polymer-encapsulated samples. The overcoat forms on the NC by interdigitating the hydrophobic portion of the amphiphilic polymer with the long alkyl chains of the TOPO cap, or perhaps phosphonic acid.[43] When placed in a polar solvent, the hydrophilic segment of the polymer presumably situates itself on the surface of the NC to be miscible with aqueous solutions. The study described here builds on the micellar encapsulation of semiconductor NCs using *N*-octylamine modified poly(acrylic acid) (PAA-OA) for labeling markers in cells.[9] This amphiphilic polymer presents only a carboxylic acid functionality, limiting the scope of chemical methods able to conjugate acceptor dyes. In order to access a wider variety of coupling strategies to NCs, we modified PAA-OA with 5-amino-1-pentanol, which adds hydroxyl functionality to NCs as shown in Scheme 1. In this design strategy, 40% of the acid groups in 1800 MW poly(acrylic acid) were targeted for functionalization with *N*-octylamine; an additional 40% of the acid groups were functionalized with 5-amino-1-pentanol and the remainder (20%) were left as free carboxylic acid. Water-soluble CdSe/ZnS NCs were prepared with the PAA-OA-AP polymer as shown in Scheme 2. Quantum yields as high as 50% were obtained for NCs encapsulated with PAA-OA-AP.

Proton NMR of PAA-OA-AP revealed very broad peaks presumably due to the amphiphilic nature of the polymer.[44,45] The peaks were too broad to accurately integrate or reference in order to probe the degree of side-chain coupling to the polymer backbone. Qualitative information was obtained with IR spectroscopy (Figure S1), inasmuch as amide peaks can be distinguished at 1653 cm^{-1} and 1551 cm^{-1} and the carbonyl peak can be distinguished at 1718 cm^{-1}. The amide bond of *N*-octylamine conjugated to the PAA backbone is nearly indistinguishable from an amide bond of 5-amino-1-pentanol conjugated to the backbone, and indeed, only one amide environment is present in the IR spectrum. Attempts were made to determine exact molecular weights with MALDI-TOF (matrix assisted laser desorption by ionization with time-of-flight detector) and ESI (electrospray ionization) mass spectrometry; however, the polymer was not detected regardless of the matrix used.

Gel Permeation Chromatography (GPC) gave insight to the degree of coupling. Figure S2 shows a calibration curve of five polystyrene molecular weight standards that was used to extrapolate the molecular weights of the polymer samples. By comparing the retention times of 1800 MW poly(acrylic acid), 40% octylamine-modified poly(acrylic acid), and 40% octylamine/40% 5-amino-1-pentanol modified poly(acrylic acid) against the retention times of polystyrene standards, approximate masses were found. The molecular weights estimated by GPC are given in Table S1. The increasing trend in molecular weights from PAA to the PAA-OA to the PAA-OA-AP confirmed that the degree of coupling increased. The molecular weight obtained by GPC correlates well to the weights that were expected for a

NIH-PA Author Manuscript

NIH-PA Author Manuscript

NIH-PA Author Manuscript

coupling efficiency of 100%. However, two aspects prevent us from assigning absolute molecular weight. First, the molecular weights are calibrated against a poly(styrene) standard, which has a very different structure compared to poly(acrylic acid). Second, the structures of the three polymers listed in Table S1 are disparate enough that their viscosities are likely to be different. Viscosities affect the flow rate of a polymer through a gel, which affects the retention time. Therefore, the three samples cannot be directly compared to allow for a direct calculation of the degree of coupling of the side chains. However, enough information was obtained through this technique to qualitatively conclude that *N*-octylamine and 5-amino-1-pentanol are both present as side chain groups on the polymer, and they indeed promote water-solubilization of the NCs and at the same time provide a hydroxyl group functionality.

Photophysical properties

The efficacy of energy transfer has been the chief means of characterization of NC FRET constructs. RITC was chosen to be the FRET acceptor dye because the dye has a high extinction coefficient.[46] Moreover, CdSe NCs can be easily synthesized so that their emission matches the absorption wavelength of RITC ($\lambda_{abs,max}$ = 556 nm) thereby engendering RITC as an ideal FRET acceptor for NCs. In addition, the isothiocyanate functionality is readily susceptible to nucleophilic attack by the hydroxyl group of the 5-amino-1-pentanol of the amphiphilic polymer to yield a covalently-bonded thiocarbamate conjugate. The average number of dyes conjugated to each NC was controlled through stoichiometry, and the constructs were separated from excess uncoupled dye and starting material through dialysis with 50 KDa molecular weight cutoff centrifugal filters until the filtrate was optically transparent.

The UV/VIS absorption spectra of RITC, water-solubilized unconjugated CdSe/ZnS NCs, and RITC-NC conjugates are presented in Figure 1. The absorption spectra of the conjugates indicate minimal change in the absorption spectrum of the dye upon binding to NCs. The spectra of the RITC-NC conjugates clearly exhibit the absorption characteristics of both the NC (with the broad absorption feature extending to higher energies) and RITC (with the dye first absorption feature at λ_{max} = 556 nm). The UV/VIS spectrum of each conjugate can therefore be deconstructed into the two components, and since the extinction coefficients of each chromophore at a specific wavelength can be calculated, an estimate of the RITC to NC ratio can be ascertained. Four different samples with dye to NC ratios of 12:1, 2.5:1, 0.8:1 and 0.3:1 were obtained. The emission spectra of the RITC, NC, and the RITC-NC conjugates are shown in Figure 2. The samples were excited at λ_{exc} = 350 nm, where the NC absorption is large and the RITC absorption is at a minimum. Accordingly, the choice of this excitation wavelength minimized direct excitation of the acceptor dye. As illustrated in Figure 2, the sample with the most dye conjugated (12:1) exhibits features nearly identical to the dye; only a minor CdSe emission is observed. Conversely, the emission spectrum of the sample with the least conjugation (0.3:1) resembles that of the CdSe NC. These comparative results are indicative of energy transfer, as the FRET efficiency is greater for the more conjugated sample where the spectral overlap is greatest. The blue-shift of the NC emission at low dye-loading levels is likely due to differential FRET efficiency across the NC

NIH-PA Author Manuscript

NIH-PA Author Manuscript

NIH-PA Author Manuscript

emission profile as recently demonstrated;[47–48] furthermore, the blue-shift of the dye acceptor emission is due to the narrow excitation window from the NC donor.[49]

Förster theory models the rate for this energy transfer, k_{FRET}, according to the spectral overlap between donor emission and acceptor absorption, *J*, the donor-acceptor distance, *r*, the donor radiative lifetime, τ_D and a constant *B*.

$$k_{FRET}=\frac{1}{\tau_D}\left(\frac{R_0}{r}\right)^6 \quad \text{with} \quad R_0=(B\times J\times \varphi_D)^{1/6} \quad (1)$$

where $B=\left(\frac{9000\ln(10)\kappa^2}{128\pi^5 n^4 N}\right)^{1/6}$ and $J=\int_0^\infty d\nu \frac{f_D(\nu)\varepsilon_A(\nu)}{\nu^4}$ R_0 is a characteristic distance, that is defined such that at where the rate of energy transfer is 50% at $r = R_0$.

The efficiency (*E*) of FRET, or the fraction of photons absorbed by the donor that are transferred to the acceptor, is the ratio of the transfer rate to the total decay rate of the donor modified by the number of acceptors, m, per donor site,

$$E=\frac{mR_0^6}{mR_0^6+r^6} \quad (2)$$

Thus, the efficiency of energy transfer is enhanced by increasing the number of acceptor molecules, *m*. It is important to note in a study that utilizes one donor and multiple acceptors, any distance measurement will represent a statistical average for the donor-acceptor pairs.

Using eq. 1, the critical transfer distance, R_0, between the 540-nm emitting NCs with 3% QY and RITC acceptor in water, assuming random dipole orientation and integrating the spectral overlap with Matlab, was calculated as 36 Å. This R_o falls within a typical Förster distance range of 20 – 90 Å.[50] Increasing the number of acceptor molecules, *m*, enhances the FRET efficiency as predicted by eq. 2. The sample with the most dye conjugated to the NC (12:1) exhibits almost no NC emission owing to nearly complete energy transfer from the NC to the dye.

In order to ensure that the emission spectra obtained reflected FRET instead of trivial re-absorption of the NC emission by the dye-acceptor, uncoupled mixtures of RITC and CdSe/ZnS were prepared. The isothiocyanate on the RITC was allowed to hydrolyze in water and then the solution was mixed with the NCs. The re-absorption efficiency depends on the total concentration of dye in solution, whereas the FRET efficiency requires the dye to be proximate to the NC. The absorbances of each component were matched to that of a control RITC-NC conjugate to ensure that the relative concentrations would be comparable. The RITC:NC ratio for the conjugate was calculated as 11:1 for this control experiment. Figure 3 clearly shows substantial residual NC emission in the unconjugated mixture, in contrast to the nearly exclusive emission from the dye in the conjugate. From this result, it

NIH-PA Author Manuscript

NIH-PA Author Manuscript

NIH-PA Author Manuscript

can be concluded that trivial re-absorption of NC emission by the dye cannot account for the enhanced dye emission when tethered to the NC surface.

To gain insight into the state that drives energy transfer, the NC-RITC constructs were studied by photoluminescence excitation spectroscopy (PLE). Figure 4 shows the PLE spectra collected for RITC, NC and the RITC-NC conjugates. The emission intensity was monitored at λ_{em} = 620 nm, where only the dye emits, and excitation wavelengths were scanned from 350 nm to 620 nm. If energy transfer is to occur from the NC, then high emission intensity is expected for excitation wavelengths that fall within the UV envelope owing to a broad NC absorption cross-section. Conversely, if there is no energy transfer, the excitation spectrum is expected to mirror that of the RITC absorbance spectrum, as only the excitation of the dye should be responsible for the observed emission. Excepting the sample with the greatest concentration of dye (12:1), Figure 4 reveals that there is a NC component to each PLE spectrum of the conjugates. The PLEs for the conjugates exhibit emission intensity for blue excitation wavelengths (between 350 – 500 nm) that are coincident with the NC absorption spectrum. As the ratio of dye to NC increases, the emission intensity from the NC component decreases, which is ascribed to the distribution of energy from one excited NC multiple dyes. For the highly loaded dye sample (12:1), the lack of the NC contribution to the observed emission is attributed to the NC absorbance becoming overwhelmed by the dye absorption; the emission spectra of the 12:1 RITC:NC conjugate is therefore predominantly due to direct excitation of the dye.

FRET was further characterized by time-resolved fluorescence spectroscopy. The donor (NC) lifetimes of the RITC-NC conjugates and the NC were extracted from the photoluminescence decay spectra of the NC emission and are presented in Figure S3. Because the NC emission of the conjugate with the highest dye coupling (12:1) was completely quenched, lifetime data on the donor of this particular conjugate could not be obtained. Time-resolved fluorescence decay curves (Figure S3) were fit by de-convolving a bi-exponential decay curve with the signal obtained from the instrument response. CdSe exciton recombination has been reported to be bi-exponential due to an existence of two different kinds of excitonic states, [51] with which our results are consistent. The decay curves show that the lifetimes of the NC emission in the RITC-NC conjugates are shorter than the lifetime of the emission of the unconjugated NC itself. The degree of quenching is also proportional to the number of acceptor dyes per NC, which is indicative of enhanced efficiency of energy transfer.

By examining the decay in the region where NC emission is dominant, lifetimes, the FRET rate constant and efficiency of energy transfer were calculated and are listed in Table 1. The longer lifetime component is assigned to the band edge excitonic recombination[51] and was used to calculate the *E*, *r*, and k_{FRET} using eqs. 1 and 2. More recently, it has been emphasized that Poisson distribution statistics must be considered at dye/NC ratios.[4752] Weighting the calculated distances by their Poisson probability results in only minimum changes to r, as listed in Table 1. Differences in *r* likely result in the inhomogeneity arising from the amphiphilic polymer micelle about the NC. The construct with more dyes conjugated (2.5:1) shows the highest energy transfer efficiency of 57%. Even with minimal amounts of acceptor dye conjugated to the NC surface (0.3:1), the FRET efficiency is still

NIH-PA Author Manuscript

NIH-PA Author Manuscript

NIH-PA Author Manuscript

high, on average approximately 40%. The rate of energy transfer was found to be on the order of 10^8 s^{-1}.

Conclusions

Water-soluble NCs is are obtained by modifying poly(acrylic acid) (PAA) with *N*-octylamine (OA) and 5-amino-1-pentanol (AP). The AP provides a site of conjugation by using it for nucleophilic attack on an isothiocyanate functionality of a dye. Facile conjugation of PAA-OA-AP polymer to rhodamine B isothiocyanate (RITC) engenders efficient fluorescence resonance energy transfer (FRET), even for a single dye acceptor on a single NC. The ease of the covalent conjugation of molecules to NCs with a PAA-OA-AP coating, together with efficient energy transfer, makes the NCs encapsulated with PAA-OA-AP attractive candidates for sensing applications.

Supplementary Material

Refer to Web version on PubMed Central for supplementary material.

Acknowledgments

This research was supported by the U.S. National Cancer Institute grants R01-CA126642 and by the ISN (W911NF-07-D-0004).

References

1. Jaiswal JK, Simon SM. Potentials and pitfalls of fluorescent quantum dots for biological imaging. Tr Cell Biol. 2004; 14:497–504.
2. Somers RC, Bawendi MG, Nocera DG. CdSe nanocrystal based chem–/bio–sensors. Chem Soc Rev. 2007; 36:579–591. [PubMed: 17387407]
3. Clapp AR I, Medintz L, Mattoussi H. Forster resonance energy transfer investigations using quantum-dot fluorophores. ChemPhysChem. 2006; 7:47–57. [PubMed: 16370019]
4. Bruchez M Jr, Moronne M, Gin P, Weiss S, Alivisatos AP. Semiconductor nanocrystals as fluorescent biological labels. Science. 1998; 281:2013–2016. [PubMed: 9748157]
5. Chan WC, Nie S. Quantum dot bioconjugates for ultrasensitive nonisotopic detection. Science. 1998; 281:2016–2018. [PubMed: 9748158]
6. Michalet X, Pinaud FF, Bentolila LA, Tsay JM, Doose S, Li JJ, Sundaresan G, Wu AM, Gambhir SS, Weiss S. Quantum dots for live cells, in vivo imaging, and diagnostics. Science. 2005; 307:538–544. [PubMed: 15681376]
7. Kim S, Lim YT, Soltesz EG, De Grand AM, Lee J, Nakayama A, Parker JA, Mihaljevic T, Laurence RG, Dor DM, Cohn LH, Bawendi MG, Frangioni JV. Near-infrared fluorescent type II quantum dots for sentinel lymph node mapping. Nat Biotechnol. 2004; 22:93–97. [PubMed: 14661026]
8. Gao X, Cui Y, Levenson RM, Chung LWK, Nie S. In vivo cancer targeting and imaging with semiconductor quantum dots. Nat Biotechnol. 2004; 22:969–976. [PubMed: 15258594]
9. Wu XY, Liu HJ, Liu JQ, Haley KN, Treadway JA, Larson JP, Ge NF, Peale F, Bruchez MP. Immunofluorescent labeling of cancer marker Her2 and other cellular targets with semiconductor quantum dots. Nat Biotechnol. 2003; 21:41–46. [PubMed: 12459735]
10. Alivisatos AP. The use of nanocrystals in biological detection. Nat Biotechnol. 2004; 22:47–52. [PubMed: 14704706]

NIH-PA Author Manuscript

NIH-PA Author Manuscript

NIH-PA Author Manuscript

11. McLaurin EJ, Greytak AB, Bawendi MG, Nocera DG. Two-photon absorbing nanocrystal sensors for ratiometric detection of oxygen. J Am Chem Soc. 2009; 131:12994–13001. [PubMed: 19697933]
12. Govorov AO. Enhanced optical properties of a photosynthetic system conjugated with semiconductor nanoparticles: The role of Förster transfer. Adv Mater. 2008; 20:4330–4335.
13. Yildiz I, Tomasulo M, Raymo FM. Electron and energy transfer mechanisms to switch the luminescence of semiconductor quantum dots. J Mater Chem. 2008; 18:5577–5584.
14. Pons T I, Medintz L, Wang X, English DS, Mattoussi H. Solution-phase single quantum dot fluorescence resonance energy transfer. J Am Chem Soc. 2006; 128:15324–15331. [PubMed: 17117885]
15. Goldman ER I, Medintz L, Whitley JL, Hayhurst A, Clapp AR, Uyeda HT, Deschamps JR, Lassman ME, Mattoussi H. A hybrid quantum dot-antibody fragment fluorescence resonance energy transfer-based TNT sensor. J Am Chem Soc. 2005; 127:6744–6751. [PubMed: 15869297]
16. Clapp AR I, Medintz L, Fisher BR, Anderson GP, Mattoussi H. Can luminescent quantum dots be efficient energy acceptors with organic dye donors? J Am Chem Soc. 2005; 127:1242–1250. [PubMed: 15669863]
17. Medintz IL, Clapp AR, Melinger JS, Deschamps JR, Mattoussi H. A reagentless biosensing assembly based on quantum dot-donor Forster resonance energy transfer. Adv Mater. 2005; 17:2450–2455.
18. Medintz IL, Uyeda HT, Goldman ER, Mattoussi H. Quantum dot bioconjugates for imaging, labelling and sensing. Nat Mater. 2005; 4:435–446. [PubMed: 15928695]
19. Clapp AR I, Medintz L, Mauro JM, Fisher BR, Bawendi MG, Mattoussi H. Fluorescence resonance energy transfer between quantum dot donors and dye-labeled protein acceptors. J Am Chem Soc. 2004; 126:301–310. [PubMed: 14709096]
20. Medintz IL, Clapp AR, Mattoussi H, Goldman ER, Fisher B, Mauro JM. Self-assembled nanoscale biosensors based on quantum dot FRET donors. Nat Mater. 2003; 2:630–638. [PubMed: 12942071]
21. Medintz IL, Clapp AR, Brunel FM, Tiefenbrunn T, Uyeda HT, Chang EL, Deschamps JR, Dawson PE, Mattoussi H. Proteolytic activity monitored by fluorescence resonance energy transfer through quantum-dot-peptide conjugates. Nat Mater. 2006; 5:581–589. [PubMed: 16799548]
22. Zhang CY, Yeh HC, Kuroki MT, Wang TH. Single-quantum-dot-based DNA nanosensor. Nat Mater. 2005; 4:826–831. [PubMed: 16379073]
23. Zhang F, Ali Z, Amin F, Riedinger A, Parak WJ. In vitro and intracellular sensing by using the photoluminescence of quantum dots. Anal Bioanal Chem. 2010; 397:935–942. [PubMed: 20306179]
24. Frasco MF, Chaniotakis N. Semiconductor quantum dots in chemical sensors and biosensors. Sensors. 2009; 9:7266–7286. [PubMed: 22423206]
25. Chen Z, Chen H, Hu H, Yu M, Li F, Zhang Q, Zhou Z, Yi T, Huang C. Versatile synthesis strategy for carboxylic acid-functionalized upconverting nanophosphors as biological labels. J Am Chem Soc. 2008; 130:3023–3029. [PubMed: 18278910]
26. Fernandez-Suarez M, Ting AY. Fluorescent probes for super-resolution imaging in living cells. Nat Rev Mol Cell Biol. 2008; 9:929–943. [PubMed: 19002208]
27. Liu L, Guo XH, Li Y, Zhong XH. Bifunctional multidentate ligand modified highly stable water-soluble quantum dots. Inorg Chem. 2010; 49:3768–3775. [PubMed: 20329710]
28. Yildiz I, McCaughan B, Cruickshank SF, Callan JF, Raymo FM. Biocompatible CdSe-ZnS core-Shell quantum dots coated with hydrophilic polythiols. Langmuir. 2009; 25:7090–7096. [PubMed: 19239226]
29. Kikkeri R, Lepenies B, Adibekian A, Laurino P, Seeberger PH. In vitro imaging and in vivo liver targeting with carbohydrate capped quantum dots. J Am Chem Soc. 2009; 131:2110–2112. [PubMed: 19199612]
30. Liu W, Choi HS, Zimmer JP, Tanaka E, Frangioni JV, Bawendi MG. Compact cysteine-coated CdSe(ZnCdS) quantum dots for in vivo applications. J Am Chem Soc. 2007; 129:14530–14531. [PubMed: 17983223]

NIH-PA Author Manuscript

NIH-PA Author Manuscript

NIH-PA Author Manuscript

31. Dubertret B, Skourides P, Norris DJ, Noireaux V, Brivanlou AH, Libchaber A. In vivo imaging of quantum dots encapsulated in phospholipid micelles. Science. 2002; 298:1759–1762. [PubMed: 12459582]
32. Guo W, Li JJ, Wang YA, Peng X. Conjugation chemistry and bioapplications of semiconductor box nanocrystals prepared via dendrimer bridging. Chem Mater. 2003; 15:3125–3133.
33. Kim S, Bawendi MG. Oligomeric ligands for luminescent and stable nanocrystal quantum dots. J Am Chem Soc. 2003; 125:14652–14653. [PubMed: 14640609]
34. Liu W, Howarth M, Greytak AB, Zheng Y, Nocera DG, Ting AY, Bawendi MG. Compact biocompatible quantum dots functionalized for cellular imaging. J Am Chem Soc. 2008; 130:1274–1284. [PubMed: 18177042]
35. Susumu K, Uyeda HT, Medintz IL, Pons T, Delehanty JB, Mattoussi H. Enhancing the stability and biological functionalities of quantum dots via compact multifunctional ligands. J Am Chem Soc. 2007; 129:13987–13996. [PubMed: 17956097]
36. Uyeda HT I, Medintz L, Jaiswal JK, Simon SM, Mattoussi H. Synthesis of compact multidentate ligands to prepare stable hydrophilic quantum dot fluorophores. J Am Chem Soc. 2005; 127:3870–3878. [PubMed: 15771523]
37. Clapp AR, Goldman ER, Mattoussi H. Capping of CdSe-ZnS quantum dots with DHLA and subsequent conjugation with proteins. Nat Protoc. 2006; 1:1258–1267. [PubMed: 17406409]
38. Liu W, Greytak AB, Lee J, Wong CR, Park J, Marshall LF, Jiang W, Curtin PN, Ting AY, Nocera DG, Fukumura D, Jain RK, Bawendi MG. Compact biocompatible quantum dots via RAFT-mediated synthesis of imidazole-based random copolymer ligand. J Am Chem Soc. 2010; 132:472–483. [PubMed: 20025223]
39. Murray CB, Norris DJ, Bawendi MG. Synthesis and characterization of nearly monodisperse CdE (E = S, Se, Te) semiconductor nanocrystallites. J Am Chem Soc. 1993; 115:8706–8715.
40. Hines MA, Guyot-Sionnest P. Synthesis and characterization of strongly luminescing ZnS-capped CdSe nanocrystals. J Phys Chem. 1996; 100:468–471.
41. Dabbousi BO, Rodriguez Viejo J, Mikulec FV, Heine JR, Mattoussi H, Ober R, Jensen KF, Bawendi MG. (CdSe)ZnS core-shell quantum dots: Synthesis and characterization of a size series of highly luminescent nanocrystallites. J Phys Chem B. 1997; 101:9463–9475.
42. Kubin RF, Fletcher AN. Fluorescence quantum yields of some rhodamne dyes. J Lumin. 1982; 27:455–462.
43. Kopping JT, Patten TE. Identification of acidic phosphorus-containing ligands involved in the surface chemistry of CdSe nanoparticles prepared in tri-n-octylphosphine oxide solvents. J Am Chem Soc. 2008; 130:5689–5698. [PubMed: 18393427]
44. Chen MH, Kumar R, Parmar VS, Kumar J, Samuelson LA, Watterson AC. Self-organization of amphiphilic copolymers into nanoparticles: Study by H-1 NMR longitudinal relaxation time. J Macromol Sci Pure Appl Chem. 2004; A41:1489–1496.
45. Liu XM, Yang YY, Leong KW. Thermally responsive polymeric micellar nanoparticles self-assembled from cholesteryl end-capped random poly(N-isopropylacrylamide-co-N,N-dimethylacrylamide): synthesis, temperature-sensitivity, and morphologies. J Colloid Interfac Sci. 2003; 266:295–303.
46. McHedlov-Petrosyan NO, Kholin YV. Aggregation of rhodamine B in water. Russ J Appl Chem. 2004; 77:414–422.
47. Medintz IL, Pons T, Trammell SA, Grimes AF, English DS, Blanco-Canosa JB, Dawson PE, Mattoussi H. Interactions between Redox Complexes and Semiconductor Quantum Dots Coupled Via a Peptide Bridge. J Am Chem Soc. 2008; 130(49):16745–16756. [PubMed: 19049466]
48. Pons T, Medintz IL, Sykora M, Mattoussi H. Spectrally Resolved Energy Transfer Using Quantum Dot Donors: Ensemble and Single-Molecule Photoluminescence Studies. Physical Review B. 2006; 73(24)
49. Krooswyk JD, Tyrakowski CM, Snee PT. Multivariable Response of Semiconductor Nanocrystal-Dye Sensors: The Case of pH. J Phys Chem C. 2010; 114(49):21348–21352.
50. Lakowicz, JR. Principles of Fluorescence Spectroscopy. 2. Kluwer Academic; New York, USA: 1999.

NIH-PA Author Manuscript

NIH-PA Author Manuscript

NIH-PA Author Manuscript

51. Javier A, Magana D, Jennings T, Strouse GF. Nanosecond exciton recombination dynamics in colloidal CdSe quantum dots under ambient conditions. Appl Phys Lett. 2003; 83:1423–1425.

52. Pons T I, Medintz L, Wang X, English DS, Mattoussi H. Solution-phase single quantum dot fluorescence resonance energy transfer. J Am Chem Soc. 2006; 128:15324–15331. [PubMed: 17117885]

NIH-PA Author Manuscript
NIH-PA Author Manuscript
NIH-PA Author Manuscript

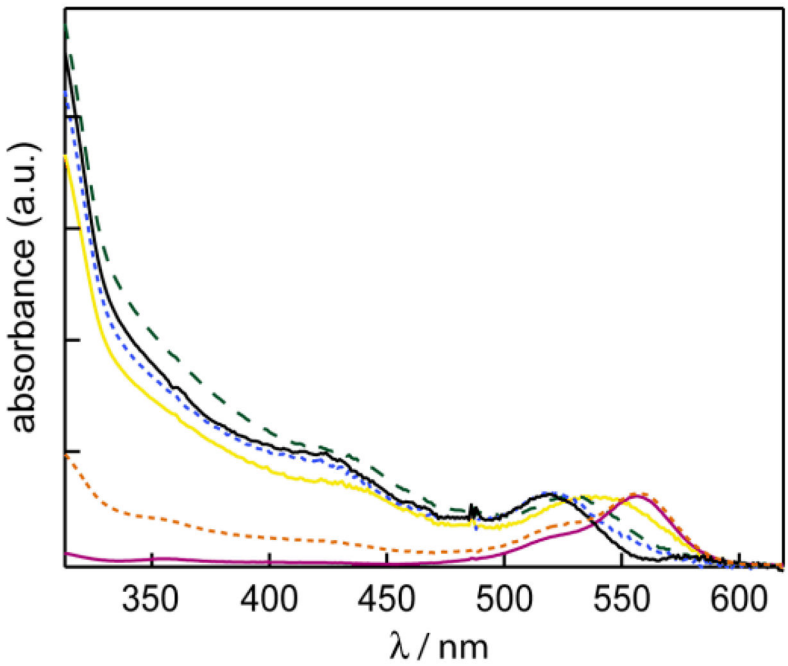

Figure 1.

UV-vis spectra of RITC (red solid line —), NC (black solid line —), and RITC-NC conjugates with RITC:NC ratio of 12:1 (orange dashed line - - -), 2.5:1 (yellow solid line —), 0.8:1 (green dashed line – – –), and 0.3:1 (blue dashed line - - -). The spectra are normalized by their first absorption feature. The small "spike" at ~480 nm is an instrumental artifact.

NIH-PA Author Manuscript
NIH-PA Author Manuscript
NIH-PA Author Manuscript

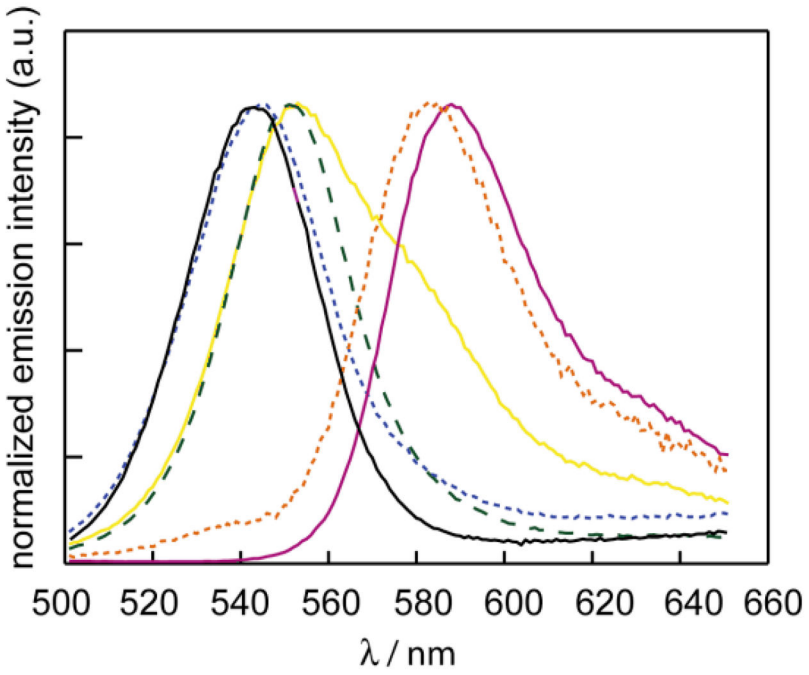

Figure 2.

Emission (λ_{ex} = 350 nm) of RITC (red solid line —), NC (black solid line —), and RITC-NC conjugates with RITC:NC ratio of 12:1 (orange dashed line - - -), 2.5:1 (yellow solid line —), 0.8:1 (green dashed line – –), and 0.3:1 (blue dashed line - - -). Where there is sufficient concentration of RITC conjugated to NC, the emission resembles RITC.

NIH-PA Author Manuscript

NIH-PA Author Manuscript

NIH-PA Author Manuscript

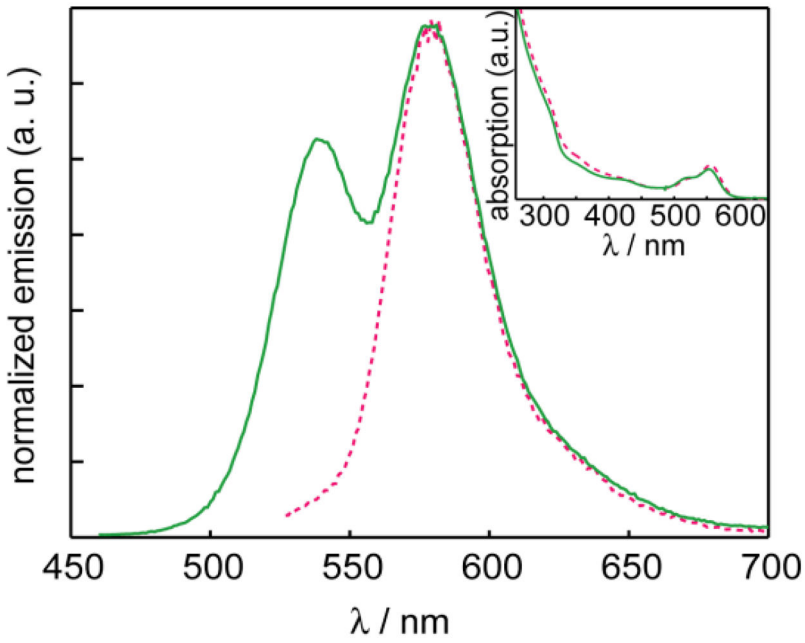

Figure 3.

Emission spectra of the mixture of NC and RITC (solid green line ——) vs. the Förster pair of the conjugated NC-RITC (red dashed line - - -), normalized by the maximum intensity of the dye emission. (Inset) The concentrations are matched by absorbance.

NIH-PA Author Manuscript
NIH-PA Author Manuscript
NIH-PA Author Manuscript

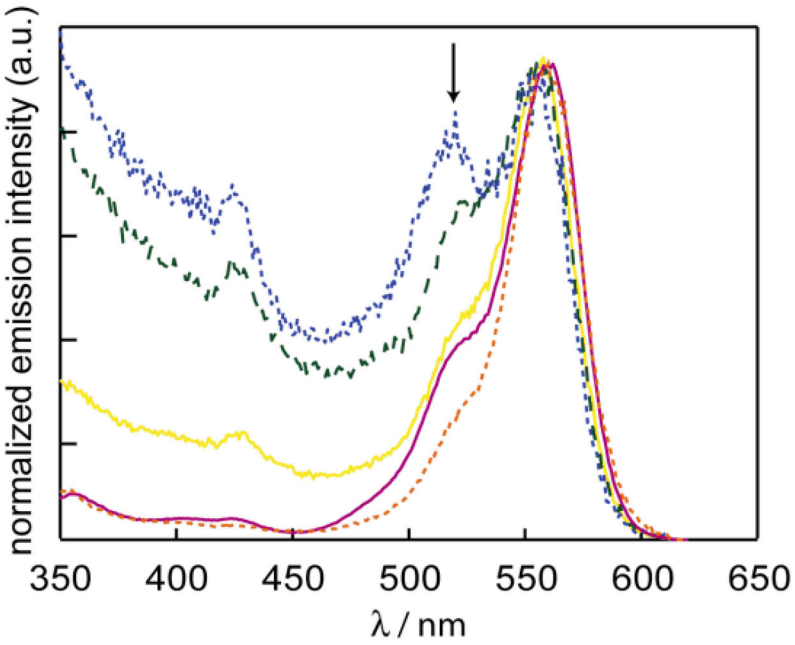

Figure 4.

PLE spectra of RITC (red solid line ——) and RITC-NC conjugates with RITC:NC ratio of 12:1 (orange dashed line - - -), 2.5:1 (yellow solid line ——), 0.8:1 (green dashed line – –), and 0.3:1 (blue dashed line - - -). The emission of each sample is scaled to the λ_{max} of dye at 583 nm to highlight the differences of each sample in the bluer wavelengths. The arrow points to the initial NC absorption feature.

NIH-PA Author Manuscript

NIH-PA Author Manuscript

NIH-PA Author Manuscript

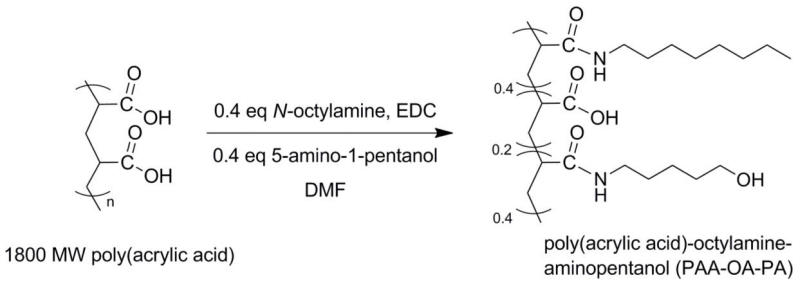

1800 MW poly(acrylic acid)

poly(acrylic acid)-octylamine-aminopentanol (PAA-OA-PA)

SCHEME 1.

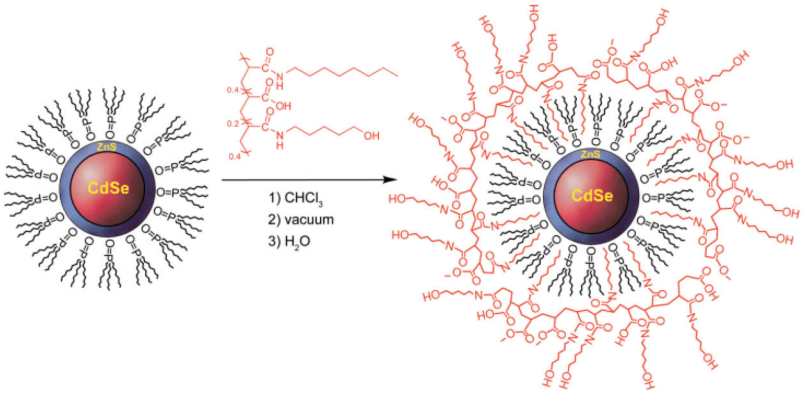

SCHEME 2.

NIH-PA Author Manuscript
NIH-PA Author Manuscript
NIH-PA Author Manuscript

NIH-PA Author Manuscript
NIH-PA Author Manuscript
NIH-PA Author Manuscript

Table 1

FRET parameters obtained from time-resolved fluorescence measurements.

Sample	RITC:NC[a]	A1[b]	$\tau_D(1)$ / ns	A2[b]	$\tau_D(2)$ / ns	r / Å[c]	E/%	k_{FRET} / s^{-1}
CdSe/ZnS NC	–	0.45	16.9	0.55	2.01	–	–	–
RITC-NC	2.5:1	0.56	6.1	0.44	0.87	38	64	1.2×10^8
RITC-NC	0.8:1	0.56	6.2	0.44	0.53	32	63	3.5×10^8
RITC-NC	0.3:1	0.49	9.2	0.51	0.12	30	45	3.0×10^8

[a] dye-to-NC ratio.

[b] pre-exponetial weighting factor of biexpoential fit.

[c] corrected for Poisson distribution statistics as discussed in ref. 52, r = 38.8 nm for the 2.5:1, r = 31.4 for 0.8, and r = 32.1 for the 0.3:1 dye/NC samples.